Tuning Conformational Structures of Imidazolium Ionenes with 1-ethyl-3-methylimidazolium Ionic Liquid Solvents

Manish Maurya,[†] Praveenkumar Sappidi,[‡] Jason E. Bara,[†] C. Heath Turner[*, †]

†Department of Chemical & Biological Engineering, The University of Alabama, Tuscaloosa, AL 35487-0203, USA

‡Department of Chemical Engineering, Indian Institute of Technology Jodhpur, Jodhpur 342037, India

***Corresponding author contact:**

E-mail: hturner@eng.ua.edu

Phone: 205-348-1733

Abstract

The structures and conformations of imidazolium ionenes solvated in 1-ethyl-3-methylimidazolium ionic liquids (ILs) ($[C_2mim^+][X^-]$) are investigated using molecular dynamics simulations. Four different ionenes poly(decylimidazolium) (PD_{10}), poly(tetraethyleneglycolimidazolium) (PE_{10}), alternating copolymer ($P(ED)_5$), and a block copolymer PE_5D_5 are immersed in $[C_2mim^+][X^-]$, where $[X^-]$ = thiocyanate $[SCN^-]$, tetrafluoroborate $[BF_4^-]$, and trifluoromethanesulfonate $[TfO^-]$. The radius of gyration indicates that the ionene chains are more extended when immersed in $[TfO^-]$ compared to $[BF_4^-]$ and $[SCN^-]$, while the solvent accessible surface area shows that PE_{10} is the most contracted ionene among all systems. The electrostatic interactions between the ionenes and the ILs are very consistent with the inherent electrostatic characteristics of the different anions, which can be quantified using the Ionic Polarity Index (IPI). The ionene configurations and dynamics strongly depend on the backbone functionality and architecture of the chain, due to the balance between the inter- and intra-molecular interactions in these systems.

Keywords: ionic liquid; ionene; imidazolium; anions; molecular dynamics

1. Introduction

Ion-containing polymers have been used as novel gas sorbents and as electrolytes in many advanced devices, such as electrochemical membranes for capacitors, lithium-ion batteries, and fuel cells.[1-6] Most of these ion-containing polymers are polyelectrolytes wherein the cation is pendant from the polymer backbone. On the other hand, in ionenes, the charge lies within the polymer backbone, which imparts a high charge density and unique electrostatic interactions.[7, 8] Ionenes provide a highly tunable material platform since different alkyl spacers can be incorporated, and the ionenes can be paired with various counterions.

Since the seminal introduction of ammonium ionenes,[9] several cation motifs have been used to form the polymer backbones, such as pyridnium,[10] phosphonium,[11] imidazolium,[12] and triazolium.[13] These ionenes possess elastomeric behavior with improved thermal and mechanical stability compared to ammonium analogs.[11, 14] Furthermore, the incorporation of ether functionality in the backbone of imidazolium ionenes has shown to improve separation and selectivity for CO_2 from gas mixtures.[15, 16] Tamami et al.[17] have shown that the charge density and the nature of the counterions tailor the thermal and rheological properties of ammonium ionenes. Hemp et al.[11] have decreased the charge density of phosphonium ionenes by increasing the length of the alkyl spacer, which in turn significantly affects the viscoelastic response of the polymer. In recent studies, the selection of counterions with different size and basicity has been explored in an effort to tune the glass transition temperature (T_g), electrospinning behavior, solubility, and thermal and structural stability of the ionenes for various applications (e.g., 3D printing, membrane fabrication, and polymer electrolytes).[18-21] In this context, Long et al.[18] have shown that polyelectrolytes with highly coordinated anions require less thermal energy to dissociate ionic interactions. Mercerreyes et al.[22] have shown that the solubility of polymerized

ionic liquids (poly(ILs)) can be tuned with different counterions through anion-exchange reactions.

Historically, imidazolium ionenes have been investigated much less than ammonium ionenes although interest in imidazolium ionenes is growing due to their similarities with imidazolium ionic liquids (ILs). Recently, Bara and co-workers.[23, 24] have synthesized imidazolium ionenes with more sophisticated architectures like polyimides and polyamides for gas separation applications. Some of these polyamide ionenes show enhanced selectivity and permeability for CO_2 relative to CH_4 and N_2 when impregnated with ILs.[24] In comparison, polyamide ionenes with consistent *para* connectivity of xylyl linkages have shown reduced gas selectivity and permeability when impregnated with ILs, as opposed to ionenes with lower chain densities and varied connectivity among the linkages. Thus, each ionene behaves differently when immersed in an IL due to the intricate balance of different inter- versus intramolecular interactions.

The introduction of an IL into the polymer matrix alters the polymer flexibility and its structure, which affects many other properties, including gas separation performance. The effects can often be unpredictable, as the impregnation of the IL can alter the interchain spacing, as well as the accessible free volume.[24] In this regard, Sappidi et al.[25] performed a series of molecular dynamics (MD) simulations and experiments to benchmark the molecular-level behavior of ionenes immersed in a 1-ethyl-3-methylimidazolium bistriflimide ($[C_2mim^+][Tf_2N^-]$) IL. It was found that the three-dimensional polymer structure (e.g., chain contraction and coiling) is strongly affected by the ionene chain functionality and its architecture, due to specific interactions with the IL solvent. In order to leverage these interactions further, multivalent imidazolium cations have been introduced as a filler in the polymer backbone to improve the gas

selectivity and permeability compared to the corresponding neat polymerized IL.[26] Despite these emerging experimental studies combining ionenes and ILs, there is still very little known about the underlying molecular-level behavior in these system, especially how the choice of the IL solvent affects the ionene conformational behavior. This information is needed for the rationale design of high-performing ionenes.

In this work, we perform a fundamental MD simulation study of the structural properties of four different imidazolium ionenes solvated in three different ILs (all with the same cation). The ionenes were chosen from those we have previously modeled and experimentally synthesized:[25] poly(decylimidazolium) (PD_{10}), poly(tetraethyleneglycolimidazolium) (PE_{10}), alternating copolymer ($P(ED)_5$), and a block copolymer (PE_5D_5), as shown in Figure 1(a). These ionenes are solvated in [C_2mim^+] ILs with three different counterions: thiocyanate [SCN^-], tetrafluoroborate [BF_4^-], and trifluoromethanesulfonate [TfO^-], as shown in Figure 1(b). Our computational analyses are used to provide a detailed understanding of the balance between the intra- and intermolecular interactions that give rise to the different three-dimensional ionene structures.

2. Computational Details

The MD simulations are performed with the GROMACS package (version 2019.4).[27] The initial configurations of the ionenes solvated within the ILs are prepared with Packmol.[28] A total of 10 repeat units of each ionene monomer are used, resulting in a net charge of +10 on the polymer. For each system, the simulation box is comprised of one ionene chain and 1000 IL molecules (i.e., 1000 cations + 1000 anions). The charge neutrality of the system is maintained by adding 10 extra anions to each system to balance the +10 ionene charge. The forcefield

parameters are taken from our previous work to model the bonded and non-bonded interactions of the ionene chain,[25] while the parameters for the ILs are derived from the OPLS-2009IL forcefield.[29] The temperature and pressure of the system are controlled using the velocity-rescaling thermostat and Berendsen barostat,[30, 31] with time constants of 0.1 and 2.0 ps, respectively. The systems are equilibrated for 140 ns in the isothermal-isobaric (NPT) ensemble at 300 K and 1 bar, and trajectories of 10 ns with a frequency of 1 ps are collected for structural analyses. A time step of 2 fs is used, while all bonds involving hydrogen atoms are constrained with the LINCS algorithm.[32] A cutoff of 1.4 nm is used for non-bonded interactions, and long-range interactions are estimated using the particle mesh Ewald (PME) method.[33] Three different independent simulations of each system are performed to generate average results and statistical analyses. The local clustering of ILs around the polymer chains is analyzed using the TRAVIS trajectory analysis tool.[34]

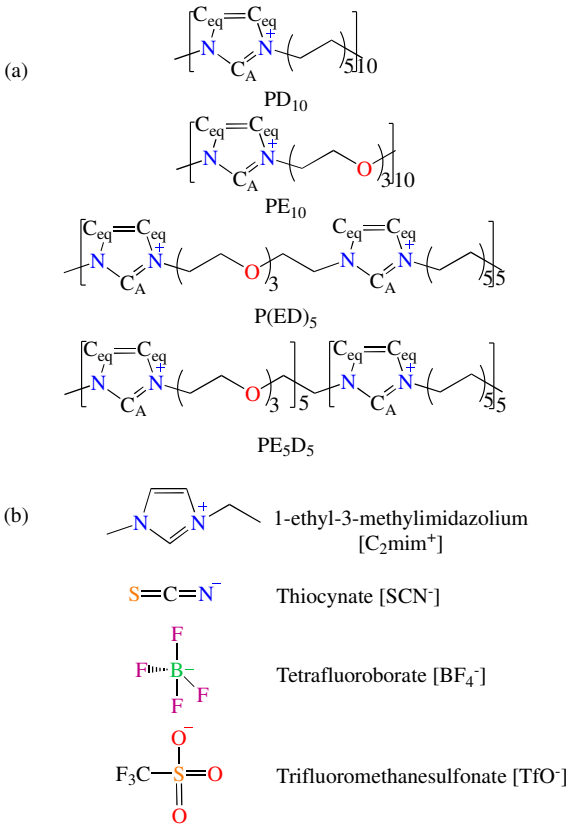

Figure 1. Schematic structure of: (a) the four different ionene chains, and (b) cation and anions of the ILs. For reference, the doubly-bonded C atoms of the imidazole ring of the ionenes are identified as C_{eq}, while the C atom between the two N atoms is the C_A site.

3. Results and Discussion

3.1 Structural and Conformational Analyses of Ionenes

The conformation structure of the ionene chains solvated with different ILs is analyzed using the radius of gyration (R_g), which is defined as:

$$\langle R_g \rangle = \sqrt{\frac{1}{N}\langle \sum_{i=1}^{N} |r(i) - r_{com}|^2 \rangle},$$

where N is the number of polymer atoms, and $r(i)$ and r_{com} are the coordinates of atom i and the center of mass, respectively. Figure 2 shows the ionene R_g values in four different ILs ([Tf_2N^-] values taken from previous work).[25] It is observed that the end-to-end distance and the angular distribution of the imidazolium rings along the ionene chains have different correlations to the R_g values. As shown in Table 1, the ionenes with larger end-to-end distances and wider angular distributions exhibit larger R_g values. Consequently, a higher R_g value is obtained for [TfO^-] compared to the smaller anions like [BF_4^-] and [SCN^-]. The maximum value of R_g (~2.43 nm) is found for PE_5D_5 in [TfO^-], and the minimum value is found for PE_{10}, regardless of the IL. Since PE_{10} has the highest density of ether groups, the strong intramolecular interactions (e.g., large, sharp peaks in the intramolecular radial distribution function presented later) lead to a more compact structure. On the other hand, $P(ED)_5$ and PE_5D_5 show wider variation in different ILs, as compared to the PD_{10} and PE_{10} systems. The R_g values of PD_{10} and the alternating ionene, $P(ED)_5$, increase in the order of [SCN^-] ≈ [BF_4^-] < [TfO^-], whereas the R_g value of the block ionene, PE_5D_5, follows the order [BF_4^-] < [SCN^-] < [TfO^-]. The difference between the R_g values of PE_{10} in different ILs is relatively small.

The trends of R_g in different ILs can be better understood with the help of Figure 3, which shows the mean-squared internal distances of the ionenes in different ILs, corresponding to the distance between atoms separated by *n* bonds along the polymer chain. The mean-squared internal distance between each bond segment is calculated and averaged over all segments, i.e., ($<R^2(n)>/n$). Figure 3(a) shows that the PD_{10} ionene is more flexible in the [TfO^-] anion as compared to the [SCN^-] and [BF_4^-] anions. Whereas the fluctuations in the ionene configuration in the [SCN^-] and [BF_4^-] anions are quite similar. The lowest chain flexibility is obtained for PE_{10}, which is also reflected in its lowest value of R_g among the other ionenes. In the case of

PE_{10}, the chain flexibility is found to be similar in each IL, as shown in Figure 3(b). In addition, we find that the conformations of the tail of the PE_{10} chain in [TfO^-] is more entangled, as compared to the [SCN^-] solvent, since the slope of the tail end of the curve is negative. Despite this, the R_g of PE_{10} in [TfO^-] and [SCN^-] are still comparable with each other. The conformational changes in alternating and block ionenes, shown in Figures 3(c) and (d), follow the same trend with respect to their R_g behavior in different ILs. The $P(ED)_5$ ionene shows an extended structure in different ILs, which is also reflected in its large end-to-end distances shown in Table 1. In the case of PE_5D_5, Figure 3(d) indicates an extended chain conformation in [TfO^-] and [SCN^-], whereas in [BF_4^-], the chain is much more contracted.

In general, we observe a different correlation between the ionene rings and the alkyl spacers/groups along the ionene chains in different ILs, as shown in Figure S1. For instance, Figure S1 shows the very strong correlation that arises in the PD_{10} system in the [SCN^-] IL solvent. These correlations can be particularly impactful on the chain entanglement, since the ionene chains are terminated with alkyl groups.

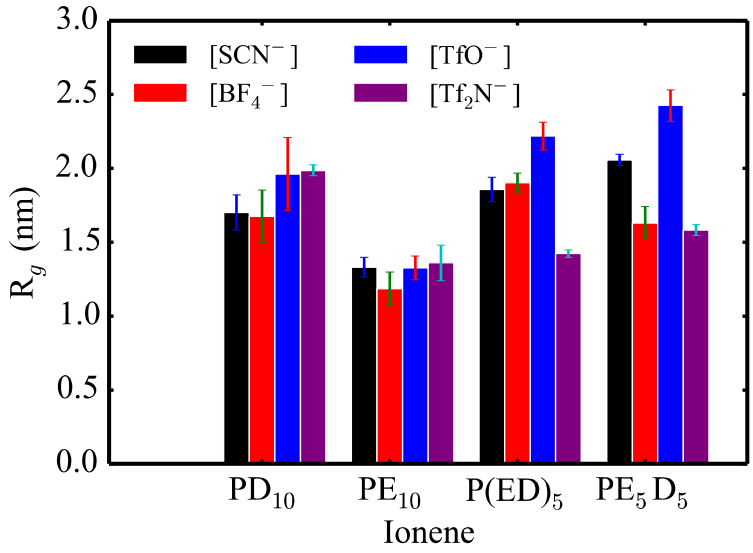

Figure 2. R_g values of the four ionenes in different ILs, labeled according to the different anion species (with a common [C_2mim^+] cation). The R_g values in [Tf_2N^-] anion from the previous work[25] is also included for comparison.

Table 1. Average angle between the C_A atoms of the imidazole rings of the ionenes and end-to-end distances.

Ionene	IL solvent	Average angle (degrees)	End-to-end distance (nm)
	[C_2mim^+][SCN^-]	109.6 ± 9.4	3.20 ± 0.4
PD_{10}	[C_2mim^+][BF_4^-]	90.2 ± 16.1	4.52 ± 1.4
	[C_2mim^+][TfO^-]	104.4 ± 12.0	4.80 ± 1.8
	[C_2mim^+][SCN^-]	100.6 ± 3.1	3.80 ± 0.8
PE_{10}	[C_2mim^+][BF_4^-]	94.4 ± 5.4	2.50 ± 0.4
	[C_2mim^+][TfO^-]	109.6 ± 3.2	2.80 ± 0.2
	[C_2mim^+][SCN^-]	121.8 ± 3.1	5.60 ± 0.6
$P(ED)_5$	[C_2mim^+][BF_4^-]	91.7 ± 15.0	6.00 ± 0.3
	[C_2mim^+][TfO^-]	111.2 ± 10.0	5.90 ± 0.3
	[C_2mim^+][SCN^-]	130.0 ± 10.0	6.20 ± 0.3
PE_5D_5	[C_2mim^+][BF_4^-]	94.4 ± 8.0	3.54 ± 0.5
	[C_2mim^+][TfO^-]	129.3 ± 3.8	6.40 ± 0.6

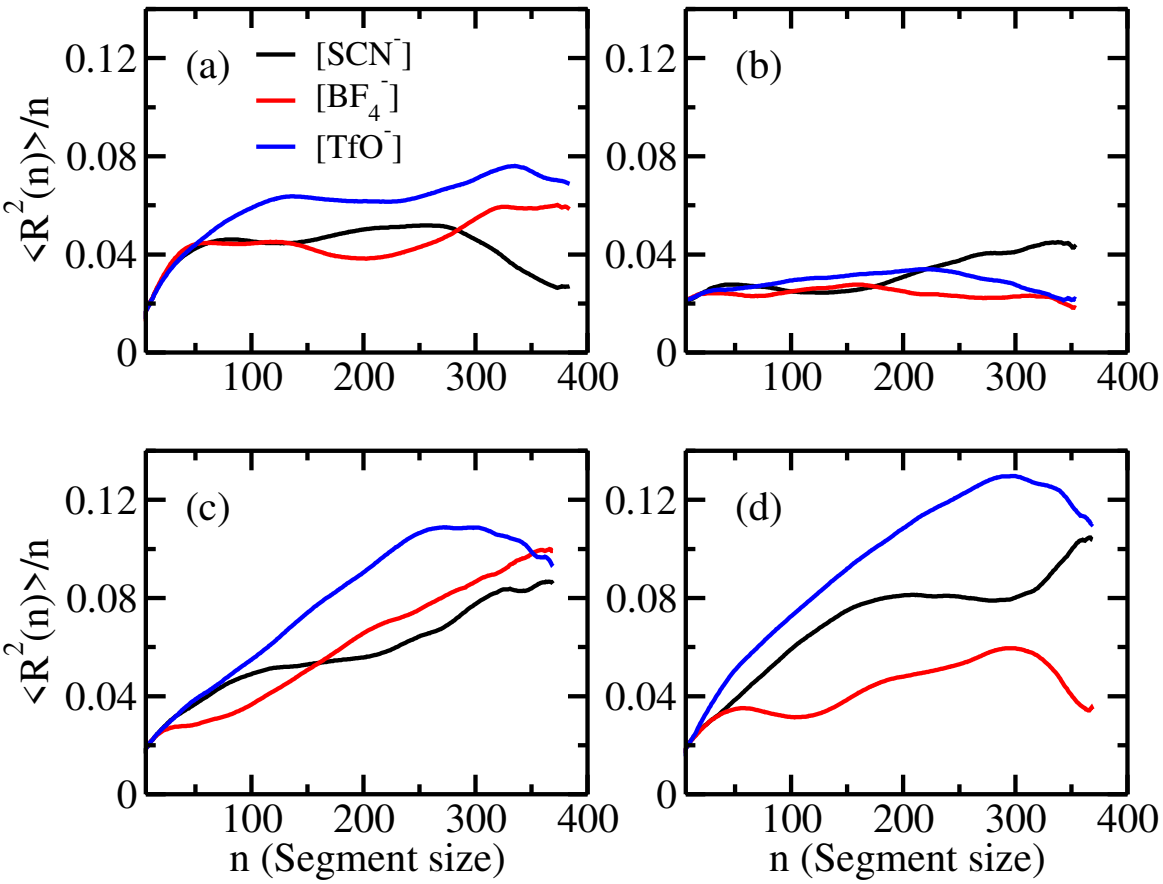

Figure 3. Mean-squared internal distances (nm^2) between atom sites within each ionene as a function of the number of bond segments separating the sites: (a) PD_{10}, (b) PE_{10}, (c) $P(ED)_5$, and (PE_5D_5) in three different ILs (with a common [C_2mim^+] cation).

Furthermore, the dihedral orientation of the ionenes immersed in different ILs are also analyzed by calculating the distribution of the dihedral angles. It is observed that the distribution of the C-C-C-C and C-C-O-C dihedral angles (shown in Figures S2 and S3, respectively) of the ionenes do not show much variability when immersed in different ILs. A very similar trend in the dihedral distribution was observed previously by Sappidi et al.[25] when these same ionenes were solvated in [C_2mim^+][Tf_2N^-].

3.2 Solvent Accessible Surface Area

The solvent accessible surface area (SASA) of the ionenes is calculated to help characterize the relative balance between the intramolecular interactions versus the interactions with the surrounding solvent molecules. Here, the SASA is defined as the area of the surface traced by the center of a probe sphere (r = 0.14 nm) rolling over the van der Waals surface of the polymer atoms, corresponding to their Lennard-Jones parameters. Table 2 summarizes the SASAs of the ionenes in different ILs. The SASA values follow the same general trends that are observed in the R_g and mean-squared internal distance analyses. The lowest values of SASA are found for PE_{10}, indicating that the chain is more contracted, along with a smaller interfacial exposure to the solvent as compared to the other ionenes. Although the ILs contain the same cation species and share other common features, the SASA values of the ionenes vary by up to 15% when exposed to different anions.

In order to more directly illustrate the connection between the SASA and the R_g values, Figure 4 provides a plot of the correlation between these two properties for all twelve systems. Although there is some variability in the relationship between SASA and R_g, there is clearly a positive linear correlation between these properties, spanning a fairly wide range of values (depending upon the specific ionene and IL combination). This is a general trend observed among different ionenes and different IL solvents, and it will be evaluated more extensively in the future with additional systems.

Table 2. Solvent accessible surface area ($Å^2$) of different ionenes.

Anions/Ionenes	**PD_{10}**	**PE_{10}**	**$P(ED)_5$**	**PE_5D_5**
[SCN^-]	3855 ± 92	3086 ± 101	3720 ± 87	3648 ± 104
[BF_4^-]	3629 ± 321	3054 ± 285	3343 ± 100	3463 ± 57

[TfO$^-$]	3883 ± 158	3062 ± 40	3694 ± 44	3954 ± 42

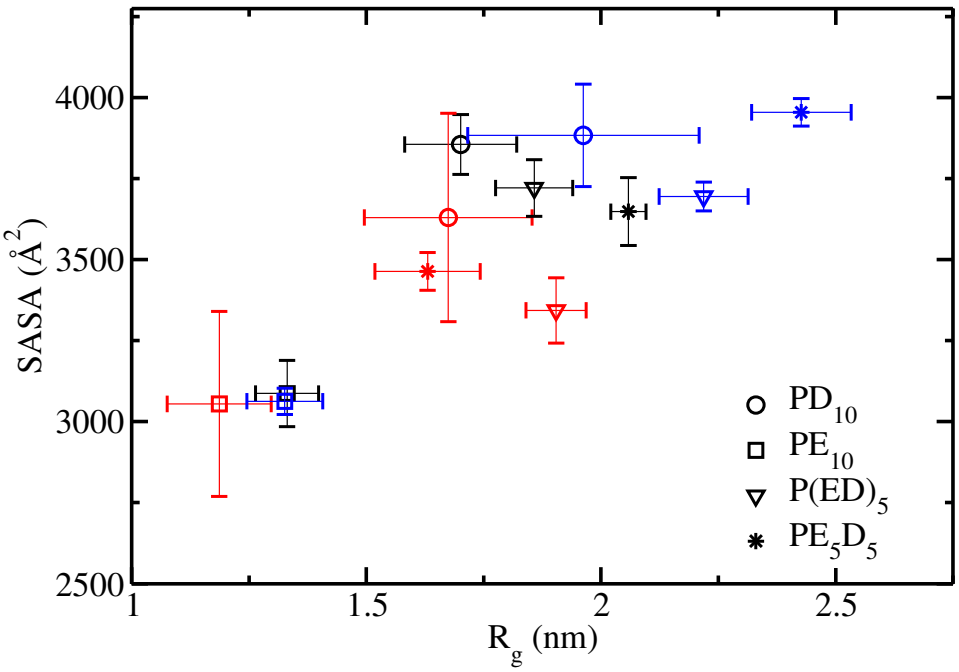

Figure 4. Change in SASA with respect to the R_g of ionene chains solvated in [SCN^-] (black), [BF_4^-] (red), and [TfO^-] (blue) anions (with a common [C_2mim^+] cation).

3.3 Electrostatic Potential Surface

While the solvation of an ionene in an IL changes the conformation of the ionene chain (leading to different R_g and SASA values), the nature of the exposed ionene surface can vary greatly. Some functional groups can be screened from interactions, while other groups can be directly exposed to the solvent environment. Here, we characterize the nature of the electrostatic interactions of the ionenes with the solvent by examining the electrostatic potential (ESP) distribution of the exposed ionene surface in the different systems. The ESP is calculated by rolling a probe atom (r = 0.14 nm) of a unit charge around the accessible surface of the ionenes,

and then the different ESP values are used to generate a statistical distribution for each ionene and IL combination. The electrostatic potential is defined as follows:

$$V = \frac{\kappa q}{r},$$

where κ is Coulomb constant, and q and r are the atomic charge on the ionene and the distance between the ionene and the probe atom, respectively.

Figure 5 shows the distribution of the ESP values, ranging from approximately -1.5 to -0.4 V. The electrostatic potential of the PD_{10} chain in Figure 5(a) shows a narrow distribution with a strong peak in [TfO^-], with an overall lower average magnitude, as compared to the [SCN^-] and [BF_4^-] anions. The ESP distributions of PE_{10} shown in Figure 5(b) indicate that PE_{10} presents a very similar electrostatic surface in all three ILs, and its average ESP magnitude is the highest among all ionenes. The similar ESP values for PE_{10} in the different ILs is also accompanied by very consistent values for both R_g and mean-squared internal distances, as shown previously. The ESP distributions for $P(ED)_5$ and PE_5D_5 show some variability in the different ILs, with relatively narrow peaks in [TfO^-], which also corresponds to average ESP values with the lowest magnitude. Among all of the ionenes, the ESP magnitude is the largest when solvated in the [BF_4^-] anion, while it is smallest when solvated in the [TfO^-] anion. This behavior is very consistent with the inherent electrostatic characteristics of the different anions. For instance, Liu et al.[35] defined the Ionic Polarity Index (IPI) as a basis for comparing the electrostatic features of different ionic species. The IPI ranking of the different anions studied here ([BF_4^-] = 123.87 kcal/mol/e; [SCN^-] = 119.27 kcal/mol/e; [TfO^-] = 104.46 kcal/mol/e) appear to have a direct effect on the ESP values of the ionenes. This provides important indications about how different IL solvents might be chosen to change the structure and properties of different ionenes.

Table 3 summarizes the mean and standard deviation of the ESP for each system, and these values are also correlated with the SASA of the ionenes, as shown in Figure 6. There is a clear trend observed, leading to an increase in the magnitude of the ESP as the SASA decreases. This is a general consolidated trend that is observed among different ionenes and different IL solvents. In other words, the electrostatic interactions between the ionenes and the IL solvent becomes more significant in the more compact ionene configurations. The maximum and the minimum values of the SASA and ESP are found in [TfO^-] and [BF_4^-], respectively.

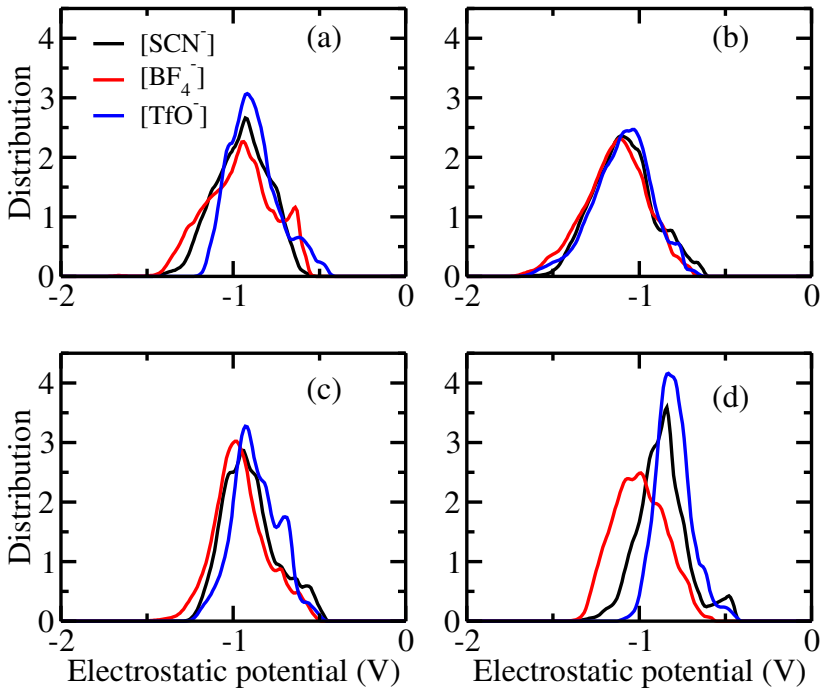

Figure 5. Distribution of the ESPs of (a) PD_{10}, (b) PE_{10}, (c) $P(ED)_5$, and (d) PE_5D_5 ionenes solvated in [SCN^-], [BF_4^-], and [TfO^-] anions (with a common [C_2mim^+] cation).

Table 3. Mean and standard deviation of the distribution of the ionene ESPs (V).

Anions/Ionenes	**PD_{10}**	**PE_{10}**	**$P(ED)_5$**	**PE_5D_5**
[SCN^-]	-0.95 ± 0.15	-1.09 ± 0.18	-0.90 ± 0.16	-0.87 ± 0.14

[BF_4^-]	-0.96 ± 0.19	-1.14 ± 0.18	-0.95 ± 0.16	-0.99 ± 0.15
[TfO^-]	-0.88 ± 0.15	-1.09 ± 0.17	-0.87 ± 0.14	-0.80 ± 0.10

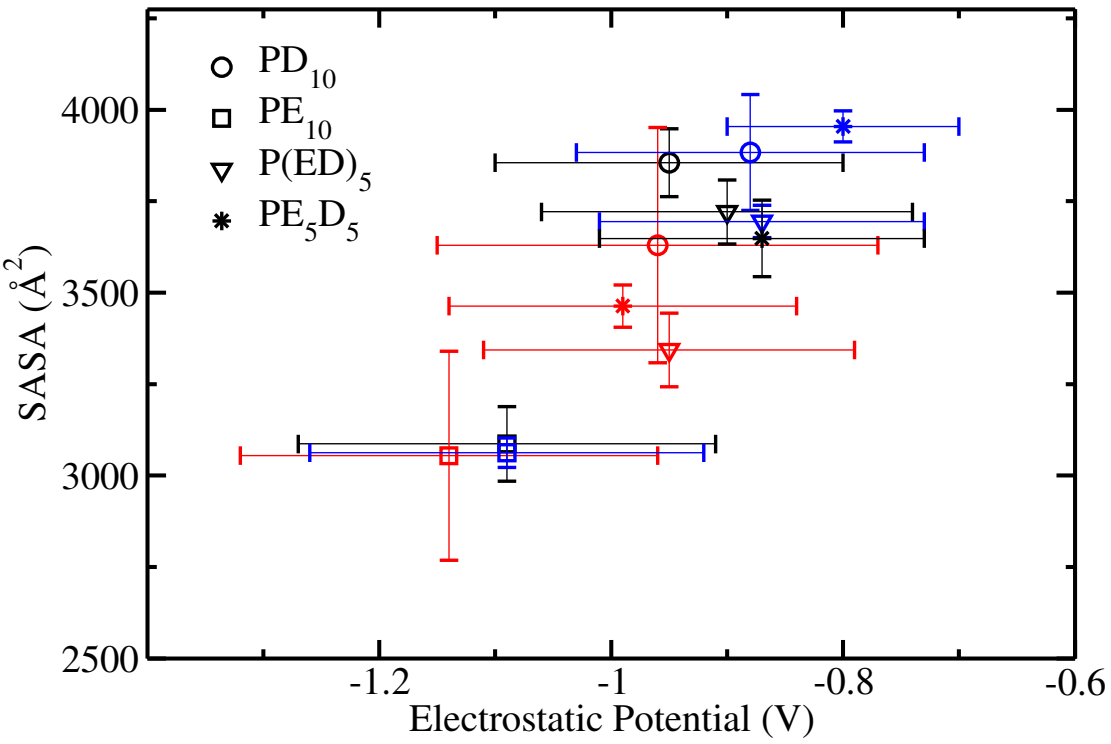

Figure 6. Variation in SASA with respect to the ESP of different ionenes solvated in [SCN^-] (black), [BF_4^-] (red), and [TfO^-] (blue) anions (with a common [C_2mim^+] cation).

3.4 Radial Distribution Functions

The specific site-site interactions in the system are analyzed by evaluating the structural correlations between different intra- and intermolecular sites in the system. Figure 7 shows the radial distribution functions (RDFs) between the intramolecular centers-of-mass of the imidazole rings ($IM_{polymer}$) along the ionene chain. Each of the twelve combinations of ionenes and ILs displays a very different RDF, but there are some trends and features worth noting. The PE_{10} ionene shows very strong correlations when solvated in [TfO^-], while the other ionenes display

the opposite behavior, with relatively weak correlations in this IL. Aside from PE_{10}, the other ionenes show relatively strong correlations in the [BF_4^-] IL, with the first peak centered at ~0.5 nm. In addition, it is observed that the ionenes show a broad first RDF peak in bulkier anions ([TfO^-] and [Tf_2N^-]).

In addition to the intramolecular RDF analyses, we have also calculated the probability density distribution of the angle formed between the ring carbon atoms (C_A) along the length of the ionene chains, as shown in Figure S6. As with the RDF analyses, the angular distributions can be somewhat different among the ionenes, but there are some trends in the distributions. For instance, the [BF_4^-] IL tends to push the distributions to lower angles as shown in Table 1, indicating less extended structures. This is consistent with R_g and SASA analyses that also reflect smaller values (more compact structures). The PE_5D_5 ionene in [TfO^-] also shows one of the highest probability distributions at the largest angles, and this is also the system that corresponds to some of the largest mean-squared internal distances, SASA, and R_g.

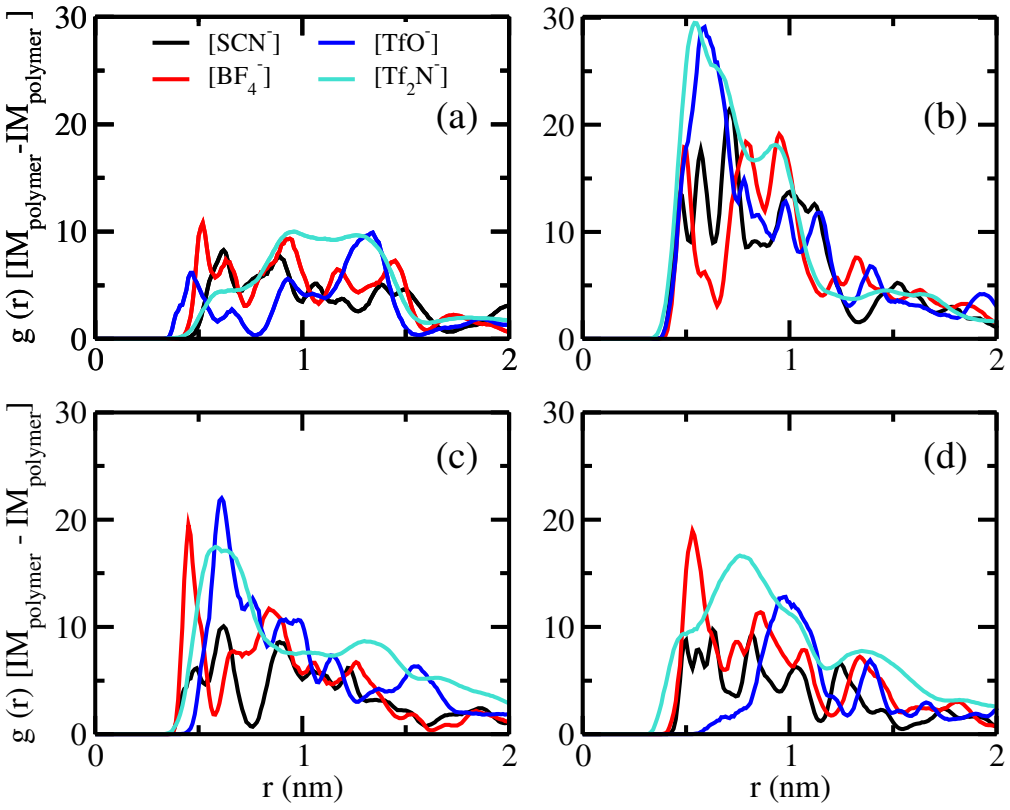

Figure 7. RDFs of the centers-of-mass of the imidazolium ring of the ionenes: (a) PD_{10}, (b) PE_{10}, (c) $P(ED)_5$, and (d) PE_5D_5 solvated in [SCN^-], [BF_4^-], [TfO^-], and [Tf_2N^-] anions (with a common [C_2mim^+] cation).

The intramolecular interactions between different ring C atoms and the O atoms of the ether groups within the ionenes are also analyzed. The ionene imidazolium rings have two equivalent carbons (C_{eq}) and a third carbon (C_A) located between the nitrogen atoms, as identified previously (Figure 1). Figure 8 presents the ether oxygen interaction with the C_A atoms, while Figure 9 presents the interactions involving the C_{eq} atoms. There are similarities in both RDF analyses, since the ionene architecture will naturally have a strong influence on these intramolecular correlations. However, it can be observed that the choice of IL has a clear influence on the $P(ED)_5$ ionene, with the strongest correlations in [TfO^-] and the weakest correlations in [SCN^-]. The IL solvent also influences the correlations in the other two ionenes, but the impact is less significant. In all systems, it appears that the [TfO^-] solvent leads to the largest correlations between the ether oxygen groups and the imidazolium carbons within the ionenes.

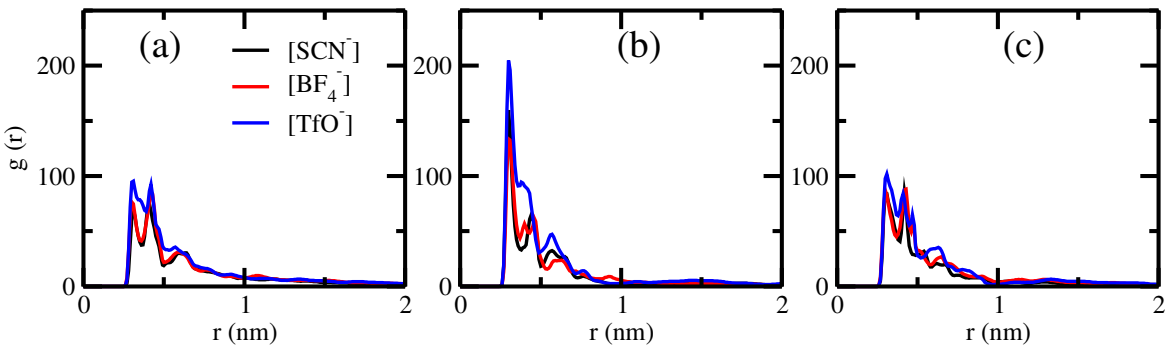

Figure 8. Intramolecular RDFs between the C_A site (identified in Figure 1) of the imidazolium rings and the ether oxygens of the ionene in different ILs (with a common [C_2mim^+] cation): (a) PE_{10}, (b) $P(ED)_5$, and (c) PE_5D_5.

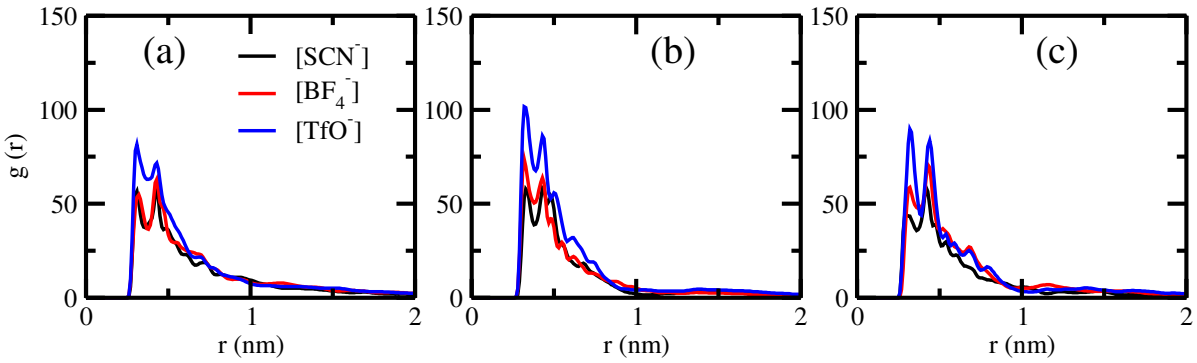

Figure 9. Intramolecular RDFs between the equivalent carbon C_{eq} (identified in Figure 1) of the imidazolium rings and ether oxygens of the ionene in different ILs (with a common [C_2mim^+] cation): (a) PE_{10}, (b) $P(ED)_5$, and (c) PE_5D_5.

Next, we investigate the intermolecular interactions between the imidazolium ring carbon atoms of the ionenes with the centers-of-mass (COMs) of the anion species, as shown in Figures 10 and 11. Figure 10(a) shows the PD_{10} RDF of the C_A site with the three ILs. The peak of the first coordination shell in [SCN^-] is found at a shorter distance than in [BF_4^-] and [TfO^-], but the intensity of the peak is smaller in [SCN^-], indicating a weaker interaction. The RDF of the C_A sites of the PE_{10} system are shown in Figure 10(b), and the results indicate that the interaction of C_A is strongest with [TfO^-]. The interaction of the C_A site with the anions decreases with the introduction of the ether groups in the ionene backbone, as compared to alkyl-substituted ionenes. However, the block ionene (PE_5D_5) shows enhanced interaction of C_A with different anions. In the case of both the alternating and block ionenes, the strongest interaction between C_A and the anions is also found for [TfO^-].

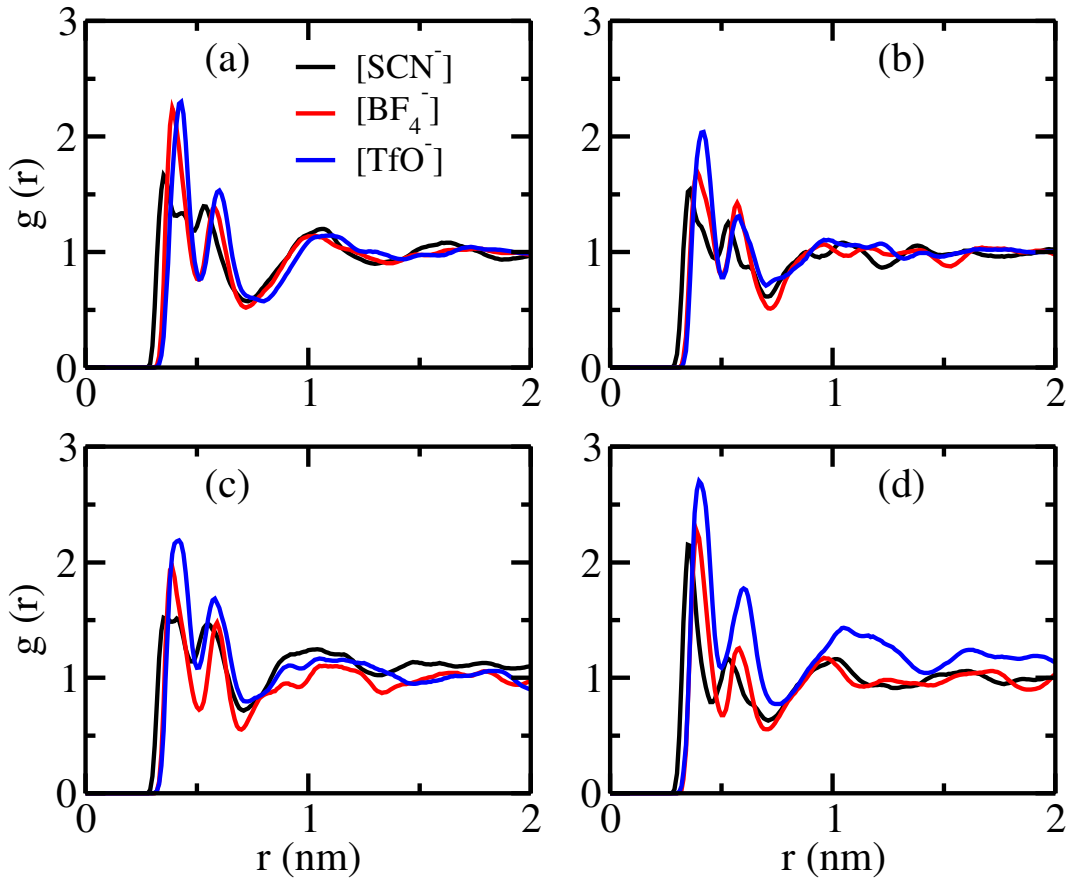

Figure 10. RDFs between the anion COMs and the C_A of the imidazole ring of the ionene in different ILs (with a common [C_2mim$^+$] cation): (a) PD_{10}, (b) PE_{10}, (c) $P(ED)_5$, and (d) PE_5D_5.

The interaction of the equivalent carbons C_{eq} of the imidazole ring with different anions is shown in Figure 11. Although there are some subtle differences, the anion interactions with the C_{eq} carbons are very similar to the C_A carbons of the ionenes. The relative order of these interactions is consistent with Figure 10, and this is not surprising, given the close proximity of these carbon sites within the ionenes.

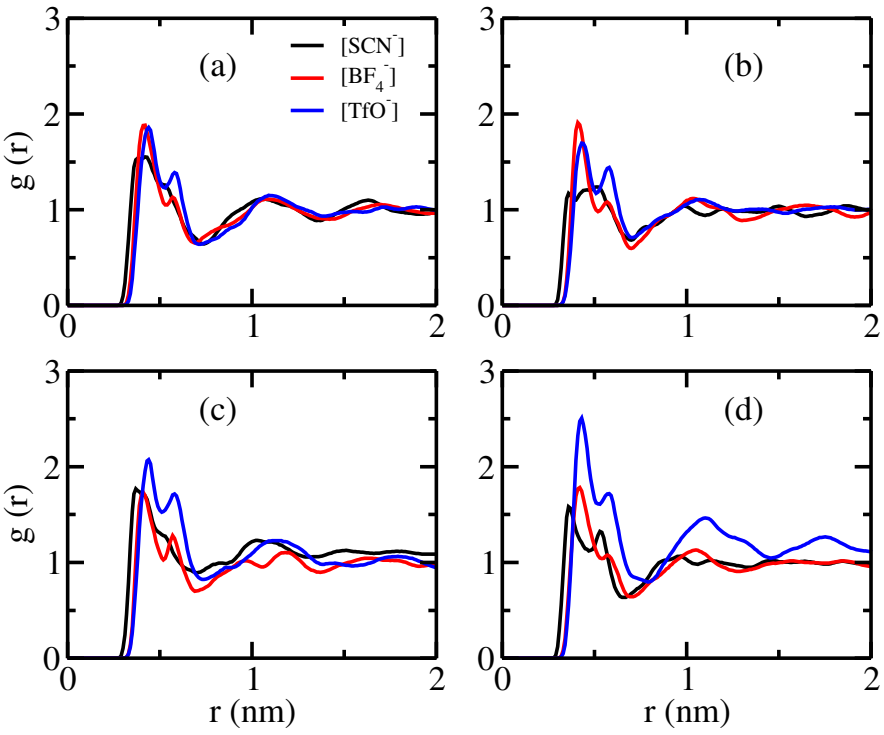

Figure 11. RDFs between anions and the C_{eq} of the imidazole ring of the ionene in different ILs (with a common [C_2mim$^+$] cation): (a) PD_{10}, (b) PE_{10}, (c) $P(ED)_5$, and (d) PE_5D_5.

Figure 12 shows the RDF between the anion COMs and the ether oxygens of the ionenes. The graph indicates that the ether oxygens of different ionene chains interact most strongly with

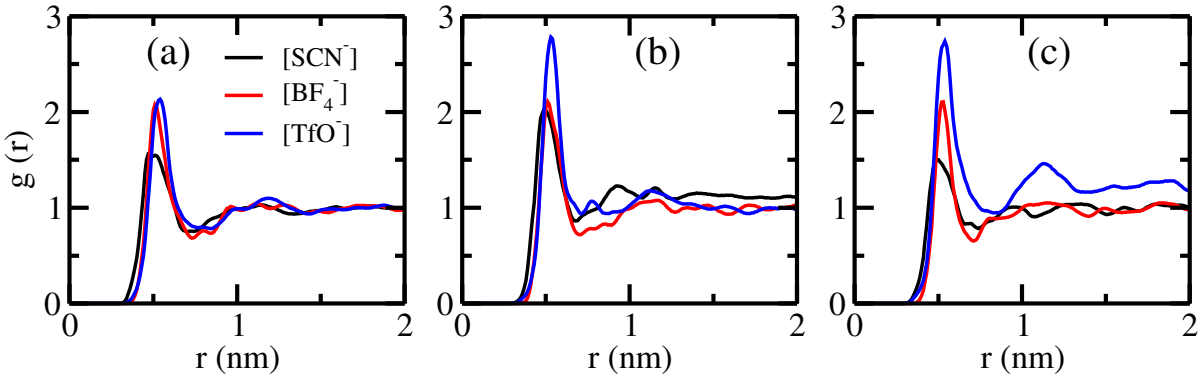

the [TfO$^-$] anion, while the weakest interaction is with [SCN$^-$]. The interaction of ether oxygen with the anions increases in alternating and block copolymers as compared to PE_{10}, especially in [TfO$^-$]. In addition to these RDF plots, the spatial distribution of the anions and cations around the imidazolium groups of the ionenes (shown in Figure S7) indicates that the anions interact more strongly with the imidazole ring.

Figure 12. RDFs between different anion COMs and the ether oxygen atoms of the ionenes in different ILs (with a common [C_2mim^+] cation): (a) PE_{10}, (b) $P(ED)_5$, and (c) PE_5D_5.

Based on the RDF analyses, we can also calculate the local coordination numbers around different sites of the ionene chains. Figure S4 shows the local coordination number of the anions around the imidazole rings of the ionenes. In contrast, the local coordination of the anions around the alkyl groups of the ionenes (Figure S5) are approximately 50% lower. Thus, the interactions between the anions and the imidazole rings of the ionenes are likely more influential in changing the overall ionene structure.

3.5 Ionene Chain Dynamics

Information about the ionene structural relaxation can be obtained by monitoring the end-to-end deviation vector correlation, which is defined as:

$$C_R(t) = \frac{\langle \delta R(t) \cdot \delta R(0) \rangle}{\langle \delta R^2 \rangle},$$

where $\delta R(t)$ is the fluctuation in end-to-end vector at time t, from its mean value $\langle \delta R \rangle$, i.e., $\delta R(t) = R(t) - \langle \delta R \rangle$.[36-39] Figure 13 displays the autocorrelation function of the four different ionenes solvated in the various ILs, and the relaxation times are very different, depending on the backbone functionality and the chain architecture. The PD_{10} chain relaxes quickly in [BF_4^-], but the dynamics are much slower in [TfO^-]. In contrast, the PE_{10} chain relaxes rapidly in [SCN^-] and becomes sluggish when solvated in [TfO^-]. The chain dynamics are not necessarily correlated to their static structural features, but there is some possible connection to the previous structural analyses. For instance, the strong intramolecular imidazolium ring correlations (Figure 7) appear to lead to slower relaxation dynamics. However, additional corroborating evidence is still needed.

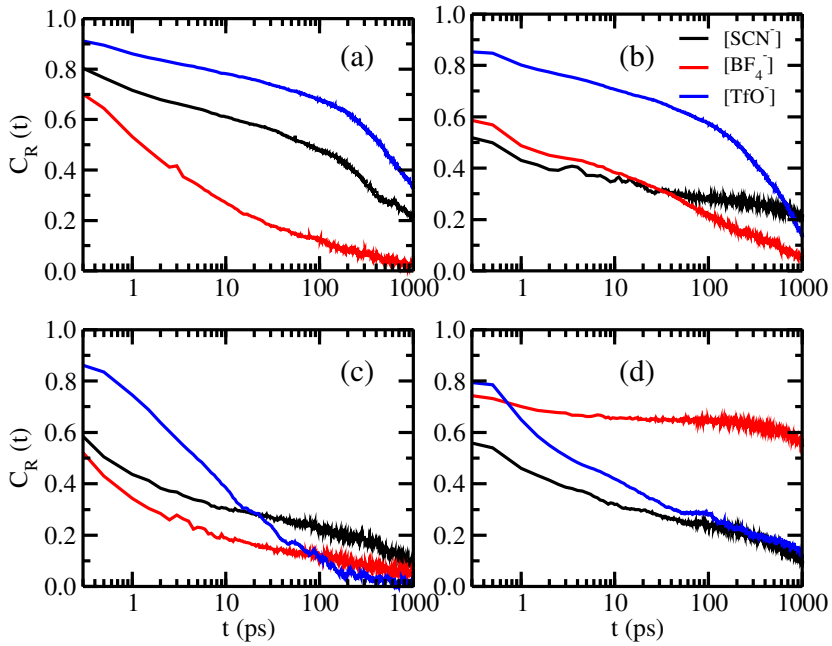

Figure 13. Time correlation function of the end-to-end fluctuation vector in different ILs (with a common [C_2mim$^+$] cation) of: (a) PD_{10}, (b) PE_{10}, (c) $P(ED)_5$, and (d) PE_5D_5.

4. Conclusions

The effects of various IL solvents ([C_2mim$^+$][SCN$^-$], [C_2mim$^+$][BF_4^-], and [C_2mim$^+$][TfO$^-$]) on the structures and conformational properties of four different imidazolium ionenes (PD_{10}, PE_{10}, $P(ED)_5$, and PE_5D_5) have been studied using MD simulations. The structures and conformations of the ionenes are found to be strongly influenced by the anion species. A comparison of the R_g and SASA values indicates that the ionene chains are more extended when immersed in [TfO$^-$] compared to [BF_4^-] and [SCN$^-$], while PE_{10} is the most contracted ionene among all systems (due to strong intramolecular interactions).

To further quantify the interactions of different ionenes with the ILs solvents, the ESP distributions of the ionenes are calculated and compared. There is a strong general correlation between the ESP and SASA values among all of these systems. The [BF_4^-] anions induce the

most negative ESP values for the ionenes, while [TFO-] tends to decrease the magnitude of the ESPs. Furthermore, the electrostatic interactions between the ionenes and the ILs are very consistent with the inherent electrostatic characteristics of the different anion molecules, which can be quantified using the IPI.

The inter- and intramolecular radial distribution functions suggest that the chain configurations of ionenes solvated in different ILs strongly depend on the backbone functionality and the type of anion used for solvation. Key interactions are found between the ionene imidazole rings and the anion species. The polymer chains are more relaxed and extended in bulkier anions compared to relatively smaller anions (i.e., higher IPI value), but the overall behavior is also related to the ionene architecture (number and arrangement of alkyl versus ether groups), since it can significantly affect the electrostatic interactions with the ILs.

Acknowledgements

This work is supported by the Alabama Advanced Solvent Cluster (AASC), funded by the U.S. Department of Energy Established Program to Stimulate Competitive Research (DOE-EPSCoR) (DE-SC0020282). We are grateful to the Alabama Supercomputer Authority for computational support.

References

1. Dong, J. M.; Zhang, Y. F.; Wang, J. Y.; Yang, Z. H.; Sun, Y. B.; Zeng, D. L.; Liu, Z. H.; Cheng, H. S., Highly porous single ion conducting polymer electrolyte for advanced lithium-ion batteries via facile water-induced phase separation process. *J Membrane Sci* **2018,** *568*, 22-29.

2. Kammakakam, I.; O'Harra, K. E.; Bara, J. E.; Jackson, E. M., Design and Synthesis of Imidazolium-Mediated Troger's Base-Containing Ionene Polymers for Advanced CO_2 Separation Membranes. *ACS Omega* **2019,** *4* (2), 3439-3448.

3. Li, M. T.; Yang, B. L.; Wang, L.; Zhang, Y.; Zhang, Z.; Fang, S. H.; Zhang, Z. X., New polymerized ionic liquid (PIL) gel electrolyte membranes based on tetraalkylammonium cations for lithium ion batteries. *J Membrane Sci* **2013,** *447*, 222-227.

4. Noonan, K. J. T.; Hugar, K. M.; Kostalik, H. A.; Lobkovsky, E. B.; Abruna, H. D.; Coates, G. W., Phosphonium-Functionalized Polyethylene: A New Class of Base-Stable Alkaline Anion Exchange Membranes. *Journal of the American Chemical Society* **2012,** *134* (44), 18161-18164.

5. Elabd, Y. A.; Hickner, M. A., Block Copolymers for Fuel Cells. *Macromolecules* **2011,** *44* (1), 1-11.

6. Mittenthal, M. S.; Flowers, B. S.; Bara, J. E.; Whitley, J. W.; Spear, S. K.; Roveda, J. D.; Wallace, D. A.; Shannon, M. S.; Holler, R.; Martens, R.; Daly, D. T., Ionic Polyimides: Hybrid Polymer Architectures and Composites with Ionic Liquids for Advanced Gas Separation Membranes. *Industrial & Engineering Chemistry Research* **2017,** *56* (17), 5055-5069.

7. Abdulahad, A. I.; Jangu, C.; Hemp, S. T.; Long, T. E., Influence of Counterion on Thermal, Viscoelastic, and Ion Conductive Properties of Phosphonium Ionenes. *Macromolecular Symposia* **2014,** *342* (1), 56-66.

8. Bara, J. E.; O'Harra, K. E., Recent Advances in the Design of Ionenes: Toward Convergence with High-Performance Polymers. *Macromol Chem Phys* **2019,** *220* (13), 1900078.

9. Gibbs, C. F.; Marvel, C. S., Quaternary Ammonium Salts from Bromopropyldialkylamines. IV. Formation of Four-Membered Rings. *Journal of the American Chemical Society* **1934,** *56* (3), 725-727.

10. Feng, D.; Wilkes, G. L.; Lee, B.; Mcgrath, J. E., Structure Property Behavior of Segmented Poly(Tetramethylene Oxide)-Based Bipyridinium Ionene Elastomers. *Polymer* **1992,** *33* (3), 526-535.

11. Hemp, S. T.; Zhang, M. S.; Tamami, M.; Long, T. E., Phosphonium ionenes from well-defined step-growth polymerization: thermal and melt rheological properties. *Polym Chem-Uk* **2013,** *4* (12), 3582-3590.

12. Williams, S. R.; Salas-de la Cruz, D.; Winey, K. I.; Long, T. E., Ionene segmented block copolymers containing imidazolium cations: Structure-property relationships as a function of hard segment content. *Polymer* **2010,** *51* (6), 1252-1257.

13. Obadia, M. M.; Drockenmuller, E., Poly(1,2,3-triazolium)s: a new class of functional polymer electrolytes. *Chem Commun* **2016,** *52* (12), 2433-2450.

14. Lee, J. S.; Hocken, A.; Green, M. D., Advances in the molecular design of ionenes for a diverse range of applications. *Molecular Systems Design & Engineering* **2021,** *6* (5), 334-354.

15. Kammakakam, I.; Rao, A. H.; Yoon, H. W.; Nam, S.; Park, H. B.; Kim, T.-H., An imidazolium-based ionene blended with crosslinked PEO as a novel polymer membrane for selective CO_2 separation. *Macromolecular Research* **2014,** *22* (8), 907-916.

16. Kanakubo, M.; Makino, T.; Taniguchi, T.; Nokami, T.; Itoh, T., CO_2 Solubility in Ether Functionalized Ionic Liquids on Mole Fraction and Molarity Scales. *ACS Sustainable Chemistry & Engineering* **2016,** *4* (2), 525-535.

17. Tamami, M.; Salas-de la Cruz, D.; Winey, K. I.; Long, T. E., Structure-Property Relationships of Water-Soluble Ammonium-Ionene Copolymers. *Macromol Chem Phys* **2012,** *213* (9), 965-972.

18. Hunley, M. T.; England, J. P.; Long, T. E., Influence of Counteranion on the Thermal and Solution Behavior of Poly(2-(dimethylamino)ethyl methacrylate)-Based Polyelectrolytes. *Macromolecules* **2010,** *43* (23), 9998-10005.

19. Marcilla, R.; Blazquez, J. A.; Fernandez, R.; Grande, H.; Pomposo, J. A.; Mecerreyes, D., Synthesis of novel polycations using the chemistry of ionic liquids. *Macromol Chem Phys* **2005,** *206* (2), 299-304.

20. O'Harra, K. E.; Kammakakam, I.; Bara, J. E.; Jackson, E. M., Understanding the effects of backbone chemistry and anion type on the structure and thermal behaviors of imidazolium polyimide-ionenes. *Polym Int* **2019,** *68* (9), 1547-1556.

21. Ye, Y. S.; Elabd, Y. A., Anion exchanged polymerized ionic liquids: High free volume single ion conductors. *Polymer* **2011,** *52* (5), 1309-1317.

22. Marcilla, R.; Alberto Blazquez, J.; Rodriguez, J.; Pomposo, J. A.; Mecerreyes, D., Tuning the solubility of polymerized ionic liquids by simple anion-exchange reactions. *Journal of Polymer Science Part A: Polymer Chemistry* **2004,** *42* (1), 208-212.

23. O'Harra, K. E.; Bara, J. E., Toward controlled functional sequencing and hierarchical structuring in imidazolium ionenes. *Polym Int* **2021,** *70* (7), 944-950.

24. O'Harra, K. E.; Kammakakam, I.; Noll, D. M.; Turflinger, E. M.; Dennis, G. P.; Jackson, E. M.; Bara, J. E., Synthesis and Performance of Aromatic Polyamide Ionenes as Gas Separation Membranes. *Membranes-Basel* **2020,** *10* (3), 51.

25. Sappidi, P.; Liu, X.; O'Harra, K. E.; Bara, J. E.; Turner, C. H., How Do Ionic Liquids "Fold" Ionenes? Computational and Experimental Analysis of Imidazolium Polymers Based on Ether and Alkyl Chain Variations Dissolved in an Ionic Liquid. *Macromolecules* **2021,** *54* (4), 1611-1622.

26. O'Harra, K. E.; DeVriese, E. M.; Turflinger, E. M.; Noll, D. M.; Bara, J. E., Design and Gas Separation Performance of Imidazolium Poly(ILs) Containing Multivalent Imidazolium Fillers and Crosslinking Agents. *Polymers-Basel* **2021,** *13* (9), 1388.

27. Abraham, M. J.; Murtola, T.; Schulz, R.; Páll, S.; Smith, J. C.; Hess, B.; Lindahl, E., GROMACS: High performance molecular simulations through multi-level parallelism from laptops to supercomputers. *SoftwareX* **2015,** *1-2*, 19-25.

28. Martínez, L.; Andrade, R.; Birgin, E. G.; Martínez, J. M., PACKMOL: a package for building initial configurations for molecular dynamics simulations. *Journal of computational chemistry* **2009,** *30* (13), 2157-2164.

29. Doherty, B.; Zhong, X.; Gathiaka, S.; Li, B.; Acevedo, O., Revisiting OPLS Force Field Parameters for Ionic Liquid Simulations. *Journal of Chemical Theory and Computation* **2017,** *13* (12), 6131-6145.

30. Bussi, G.; Donadio, D.; Parrinello, M., Canonical sampling through velocity rescaling. *The Journal of Chemical Physics* **2007,** *126* (1), 014101.

31. Berendsen, H. J.; Postma, J. v.; van Gunsteren, W. F.; DiNola, A.; Haak, J. R., Molecular dynamics with coupling to an external bath. *Journal of Chemical Physics* **1984,** *81* (8), 3684-3690.

32. Hess, B.; Bekker, H.; Berendsen, H. J.; Fraaije, J. G., LINCS: a linear constraint solver for molecular simulations. *Journal of Computational Chemistry* **1997,** *18* (12), 1463-1472.

33. Darden, T.; York, D.; Pedersen, L., Particle mesh Ewald: An N·log (N) method for Ewald sums in large systems. *Journal of Chemical Physics* **1993,** *98* (12), 10089-10092.

34. Brehm, M.; Thomas, M.; Gehrke, S.; Kirchner, B., TRAVIS—A free analyzer for trajectories from molecular simulation. *Journal of Chemical Physics* **2020,** *152* (16), 164105.

35. Liu, X.; O'Harra, K. E.; Bara, J. E.; Turner, C. H., Screening Ionic Liquids Based on Ionic Volume and Electrostatic Potential Analyses. *The Journal of Physical Chemistry B* **2021,** *125* (14), 3653-3664.

36. Freire, J. J.; Adachi, K., End-to-End Vector Correlation Function in Many-Chain Systems. *Macromolecules* **1995,** *28* (13), 4747-4749.

37. McQuarrie, D. A.; A, M. Q. D., *Statistical Mechanics*. Harper & Row: New York: 1975; p Ch. 21.

38. Chandler, D., Introduction to modern statistical mechanics. Oxford University Press: New York, 1987; p Ch. 8.

39. Maurya, M.; Metya, A. K.; Singh, J. K.; Saito, S., Effects of interfaces on structure and dynamics of water droplets on a graphene surface: A molecular dynamics study. *The Journal of Chemical Physics* **2021,** *154* (16), 164704.

Graphical Abstract